Surface solar radiation trends over Europe assessed from ground-based measurements and satellite imagery and their comparison with climate models

L. C. Segado-Moreno[1] J. A. Ruiz-Arias[2] J. P. Montávez[1]

[1]Physics of the Earth, Regional Campus of International Excellence (CEIR) "Campus Mare Nostrum", University of Murcia, Spain.

[2]Department of Applied Physics I, University of Málaga, Málaga, Spain

EGU General Assembly 2023
Vienna, Austria, April 25, 2023

1. Introduction

- Downward surface solar radiation (**SSR**) is the **main component** of the surface **energy budget**.
- SSR sustains a large number of natural processes and is the **fundamental source** of energy in various forms of **solar thermal** and **photovoltaic** technologies.
- Changes in SSR can have profound environmental, social and economic implications.

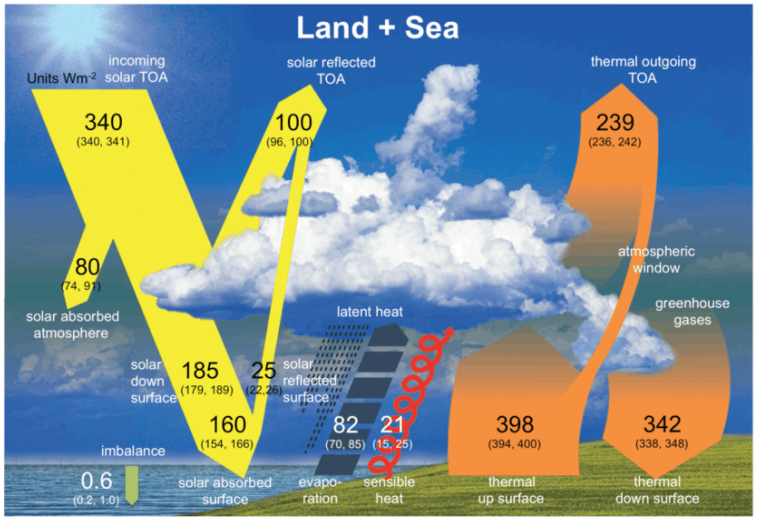

Figure: Schematic diagram of the Earth's global annual average energy balance (Wild et al., 2015).

1. Introduction

Figure: Pyranometer, used to measure Global Horizontal Irradiance (GHI), also known as SSR.

- **Ground-based observations** have been the most reliable data source for SSR monitoring.
- However, multi-decadal **stations** are **scarce** and located only in specific regions.

1. Introduction

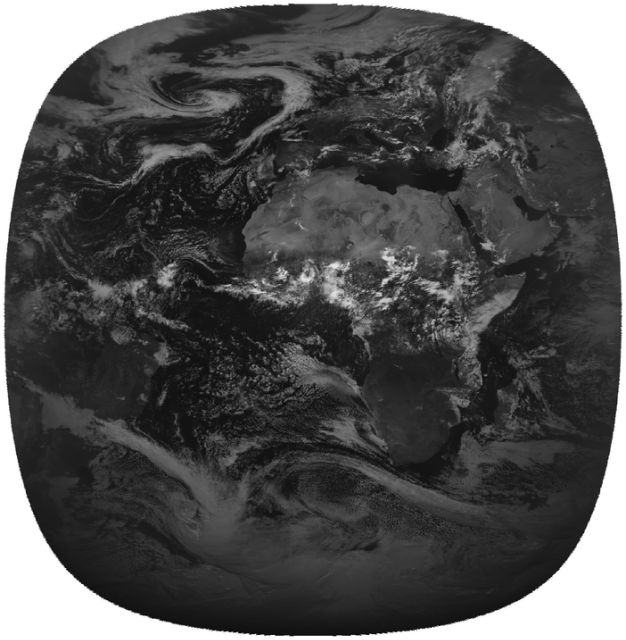

Figure: Satellite image in the visible spectrum, obtained by the SEVIRI (Spinned Enhanced Visible and InfraRed Imager) device on board the Meteosat Second Generation (MSG). Source: Eumetsat[1].

- At monthly scale, the uncertainty of **satellite-based estimates** can be comparable to that of ground sensors[2], with the additional benefit that they are **spatially continuous**[3].
- This approach has already been considered by previous studies[4].

[1] `https://navigator.eumetsat.int/start`.
[2] Perez et al. (2017)
[3] With a nominal spatial resolution of $\approx$ 5 km, or finer.
[4] Pfeifroth et al. (2018); Pinker et al. (2005); Sanchez-Lorenzo et al. (2013, 2017).

In summary, this work has two main objectives:

[5] Lee et al. (2022).

In summary, this work has two main objectives:

1. Determining the **capability** of the satellite-based SSR estimations to reproduce surface measurements.

[5] Lee et al. (2022).

In summary, this work has two main objectives:

1. Determining the **capability** of the satellite-based SSR estimations to reproduce surface measurements.

2. **The evaluation of the long-term trends** of SSR in Europe:
   - During the study period from **1994 to 2019**.
   - For the forthcoming decades **up to 2050** based on results of Coupled Model Intercomparison Project Phase 6 (**CMIP6**) climate model runs under **multiple SSP** scenarios[5].

[5] Lee et al. (2022).

Ground-based dataset

SSR measurements used in this study are a **subset** of the Global Energy Balance Archive[6](**GEBA**) over Europe.

Maintained by the Institute for Climate and Atmospheric Sciences at the ETH Zurich[7].

Contains **monthly averages** of various energy flux components, including more than 2,500 locations and 500,000 monthly average values.

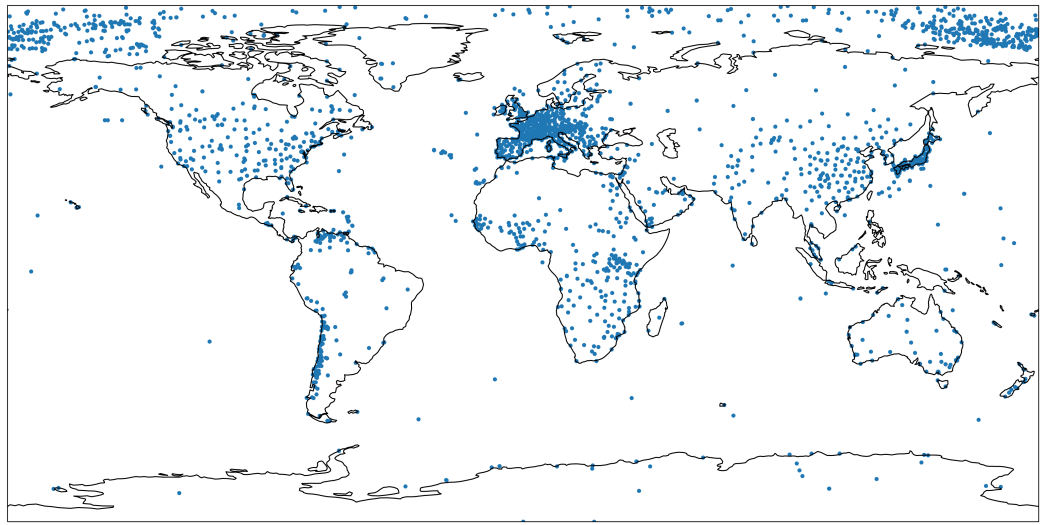

Figure: Spatial distribution of the GEBA SSR measurement stations.

[6] Gilgen et al. (1998); Gilgen and Ohmura (1999); Wild et al. (2017).
[7] `http://www.geba.ethz.ch/`

2. Data

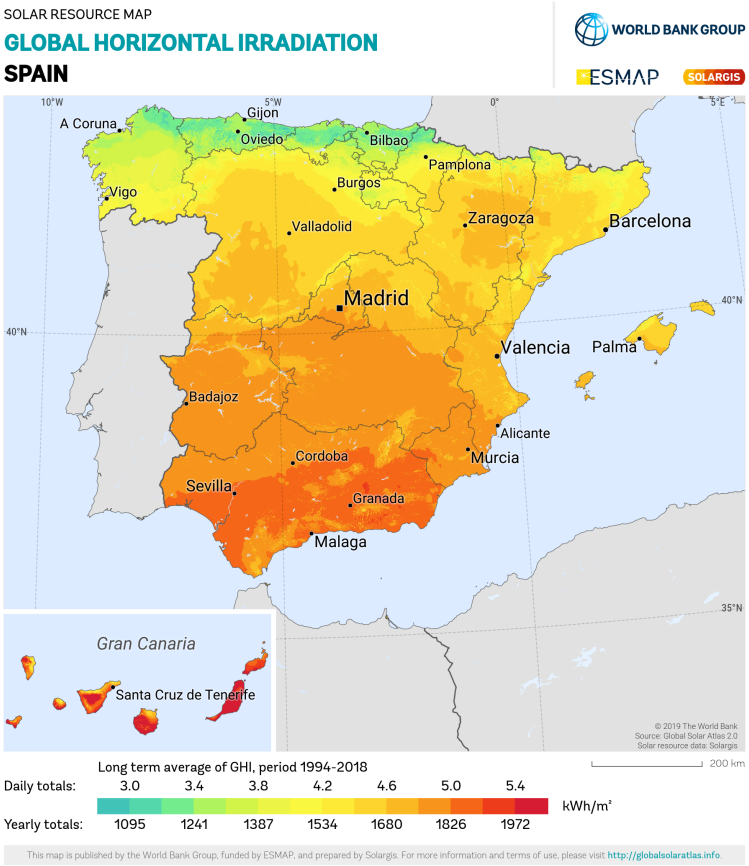

Figure: Cumulative global horizontal irradiance (GHI) map over Spain, provided by Solargis.

Satellite-based dataset

Satellite-based SSR data belong to the high-resolution **Solargis** database[8].

Built and operated by the Solargis company[9], SSR database is **generated with a proprietary model** that integrates satellite imagery and weather model outputs.

The Solargis SSR product has undergone multiple validations, proving an **outstanding performance**[10].

[8] Šúri and Cebecauer (2014).
[9] `https://solargis.com`
[10] Ineichen (2013); Global Solar Atlas (2019).

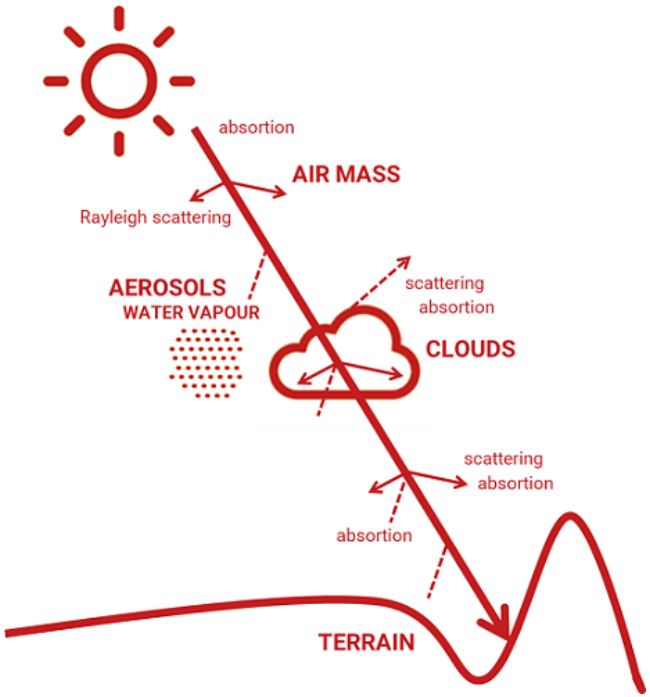

Figure: SSR estimation model scheme. Source: `https://dev.globalsolaratlas.info/support/methodology`.

Satellite-based dataset

Employs **satellite imagery** from the **MFG** (1994-2005) and **MSG** (2005 onwards).

Aerosol extinction is updated daily using AOD from various atmospheric models[11].

Thus, this dataset has the important **advantage** over previous studies[12] that it already **includes the aerosol impact on the SSR trend**.

[11] MERRA-2 (1994-2002); MACC-II (2003-2012); CAMS (2013-onwards).
[12] Pfeifroth et al. (2018); Sanchez-Lorenzo et al. (2017).

Other datasets

The **CMIP6 dataset** (Eyring et al., 2016) involves several independent climate models that quantify the **impact** of standardized **forcing pathways on climate** variables, including SSR.

We have employed SSR average series of **6 CMIP6 different models**, composed of historical series (1994-2014) and projections (2015-2050) under 4 different SSP scenarios (SSP1-2.6, SSP2-4.5, SSP3-7.0 and SSP5-8.5)

In addition, SSR data from the ECMWF **ERA5 reanalysis** (Hersbach et al., 2020) have been also considered.

2.1 Selection of GEBA sites

Selected GEBA stations meet the following **criteria**:

2.1 Selection of GEBA sites

Selected GEBA stations meet the following **criteria**:

1. Latitude is **60°** **or lower**.

2.1 Selection of GEBA sites

Selected GEBA stations meet the following **criteria**:

1. Latitude is **60°** **or lower**.
2. **Minimum** number of valid month data of **240 months** (i.e., 20 equivalent years).

2.1 Selection of GEBA sites

Selected GEBA stations meet the following **criteria**:

1. Latitude is **60°** **or lower**.
2. **Minimum** number of valid month data of **240 months** (i.e., 20 equivalent years).
3. **Minimum distance** between stations of **50 km** to prevent collinearity issues.

2.1 Selection of GEBA sites

Selected GEBA stations meet the following **criteria**:

1. Latitude is **60°** **or lower**.
2. **Minimum** number of valid month data of **240 months** (i.e., 20 equivalent years).
3. **Minimum distance** between stations of **50 km** to prevent collinearity issues.

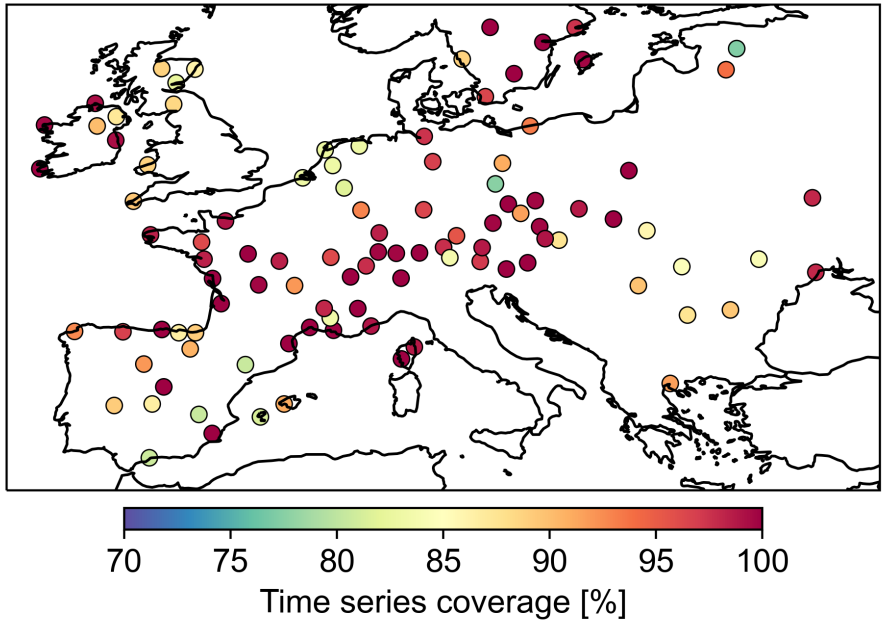

Figure: Pre-selected GEBA sites. The color shows the coverage factor (%), i.e., the fraction of valid month data in the period 1994-2019.

Under these criteria, a total of **102 stations** were originally **pre-selected**.

2.1 Selection of GEBA sites

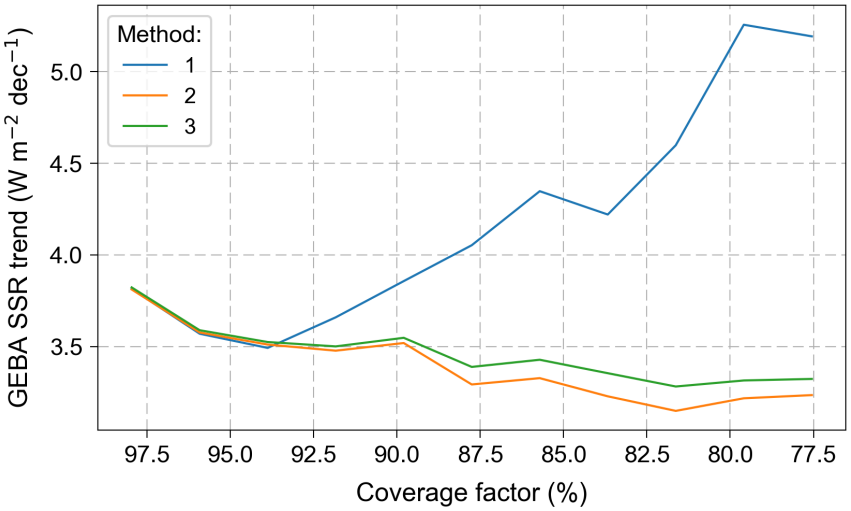

Figure: Region-wide average trend for the GEBA dataset versus minimum time series coverage factor.

- However, **data gaps** may lead to **unrealistic** average SSR series and trend values.
- The calculation of the region-wide SSR trend was performed with **3 different methods**.

- Results suggest that **methods 2 and 3 are robust** against coverage factor.
- A **minimum coverage factor of 92%** (288 months) was set.
- As a consequence, final selection of GEBA sites was reduced to **64 locations**.

2.1 Selection of GEBA sites

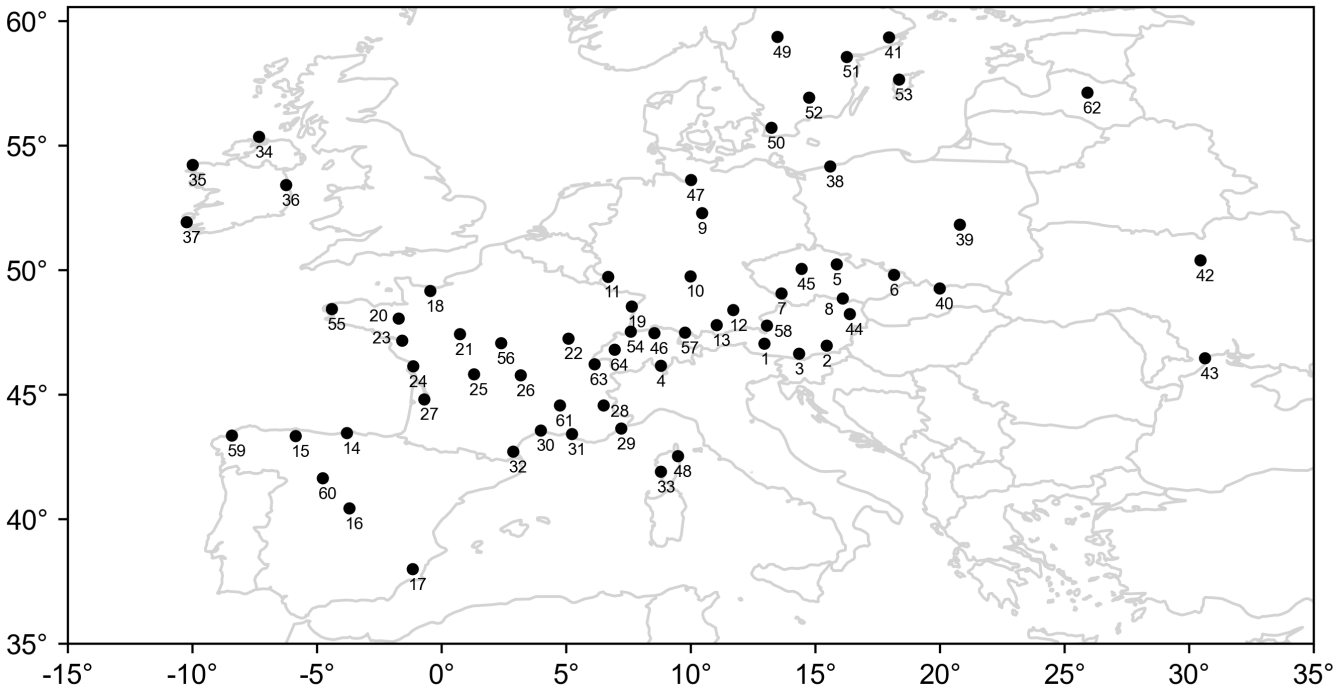

Figure: Selected GEBA station sites. All stations at these sites have a coverage factor of at least 92% and the distance between them is greater than 50 km.

For the satellite and NWP datasets, the monthly SSR values are **bilinearly interpolated** from their native spatial grid to the GEBA **station locations**.

Trend calculation

For the calculation of the **wide-area SSR trend** over separate-site trend maps and average series, **methods 2 and 3 have been used**, respectively.

Statistical significance of the trends was asserted with the **Mann-Kendall test** at a 95% confidence level (Kendall, 1948)

Error metrics

Modelled datasets were compared against the GEBA observations using **MBE, SD and RMSE** metrics.

Deseasonalised anomalies

The deseasonalised time series of anomalies have been obtained by **subtracting** from each monthly value the **average of all values for the same month**.

Homogeneity test

Possible inhomogeneities in the model datasets were detected using the **PELT algorithm** (Wambui et al., 2015) and corrected before any analysis was performed.

3.1 Homogenization of modelled datasets

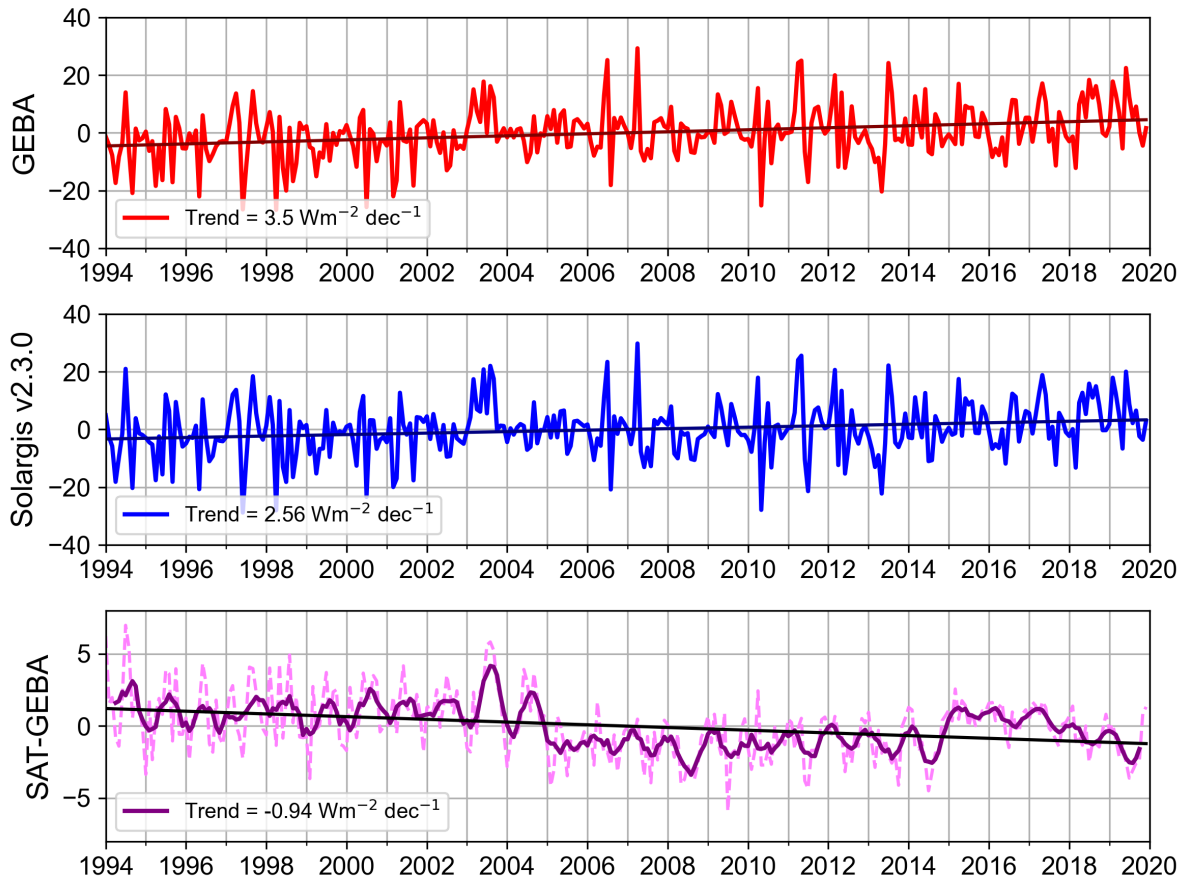

Figure: Mean monthly ground-observed (up), satellite derived (center) and residual (down) anomaly SSR series for the 1994-2019 period.

Trend mismatch between observations and satellite datasets is mainly related to these **bias inhomogeneities**.

4. Validation of modelled datasets

Table: Error metrics (MBE, RMSE and SD) obtained for the satellite derived, ERA5 and average CMIP6 datasets. Units are Wm^{-2}.

Dataset	MBE $\pm \sigma$	RMSE $\pm \sigma$	SD $\pm \sigma$
SGv2.3.0	-0.003 $\pm$ 4.187	7.657 $\pm$ 4.418	76.893 $\pm$ 7.029
ERA5	4.699 $\pm$ 6.023	11.902 $\pm$ 4.750	77.071 $\pm$ 5.997
CMIP6	7.618 $\pm$ 7.882	21.935 $\pm$ 5.067	82.059 $\pm$ 5.654

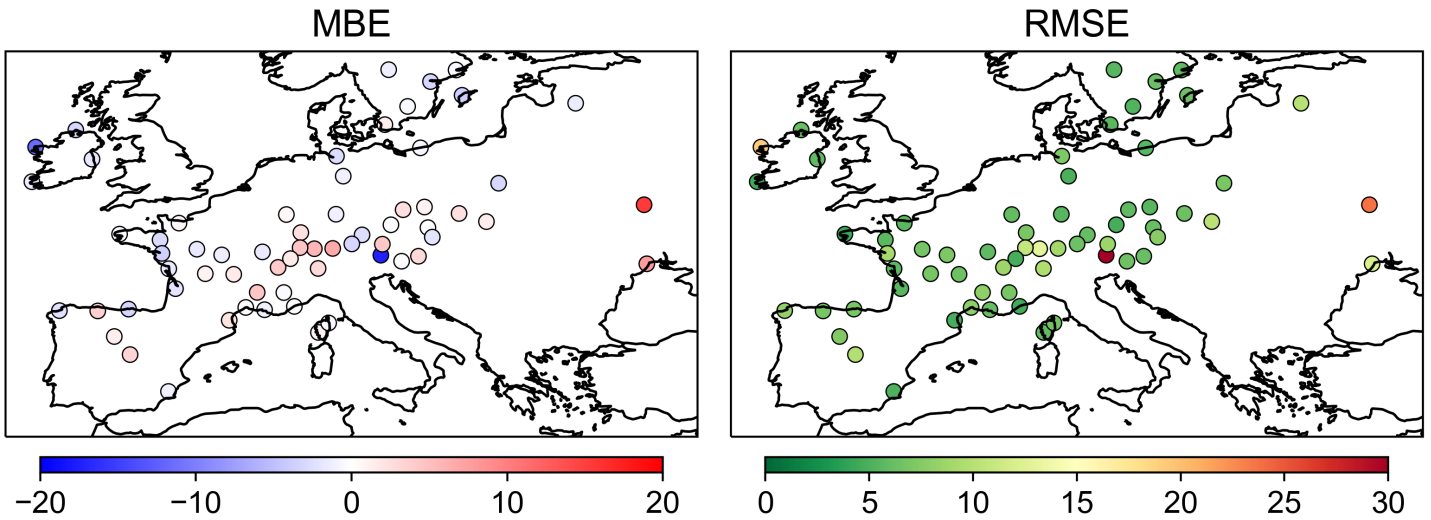

Figure: Mean Bias Error (left) and Root Mean Squared Error (right) for the Solargis dataset, for all the chosen locations, in the period 1994-2019. Units are Wm^{-2}

.

4. Validation of modelled datasets

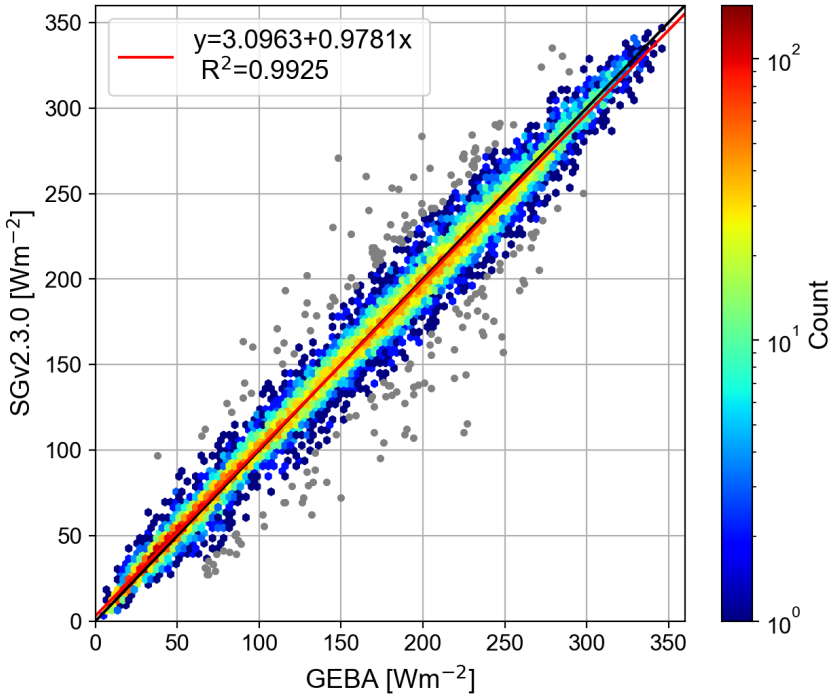

Figure: Scatter plot of satellite-estimated versus ground-based SSR measurements over the period 1994-2019. Huber robust regression method was used with a loss factor $\varepsilon = 4.5$.

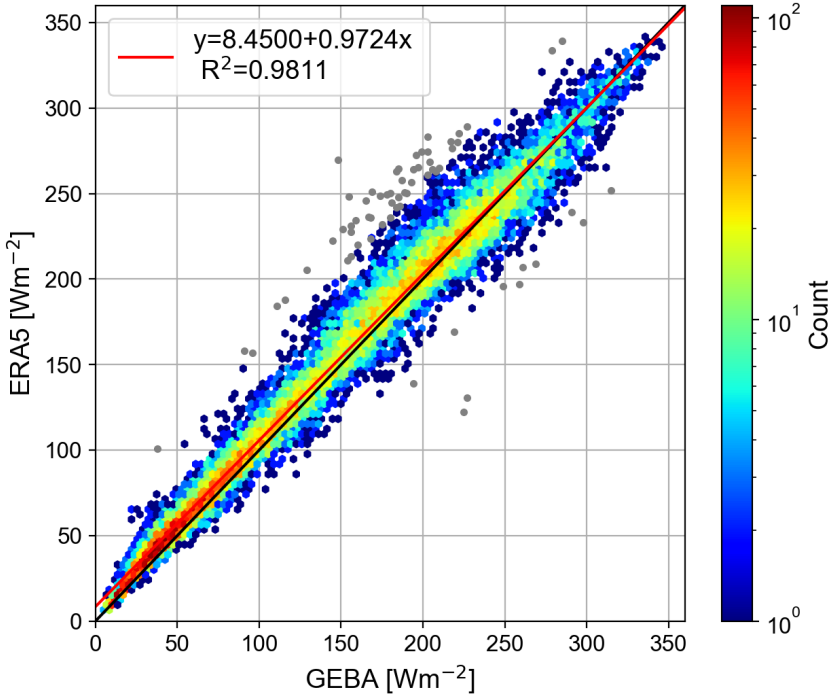

Figure: Scatter plot of ERA5 dataset versus ground-based SSR measurements over the period 1994-2019. Huber robust regression method was used with a loss factor $\varepsilon = 4.5$.

4. Validation of modelled datasets

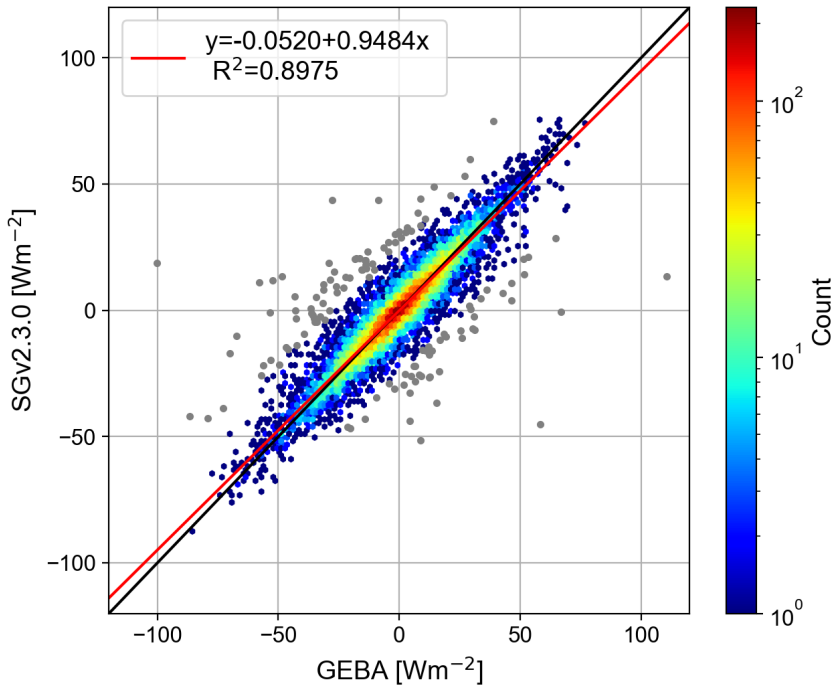

Figure: Scatter plot of satellite-estimated versus ground-based measurements of SSR deseasonalised, detrended anomalies over the period 1994-2019.

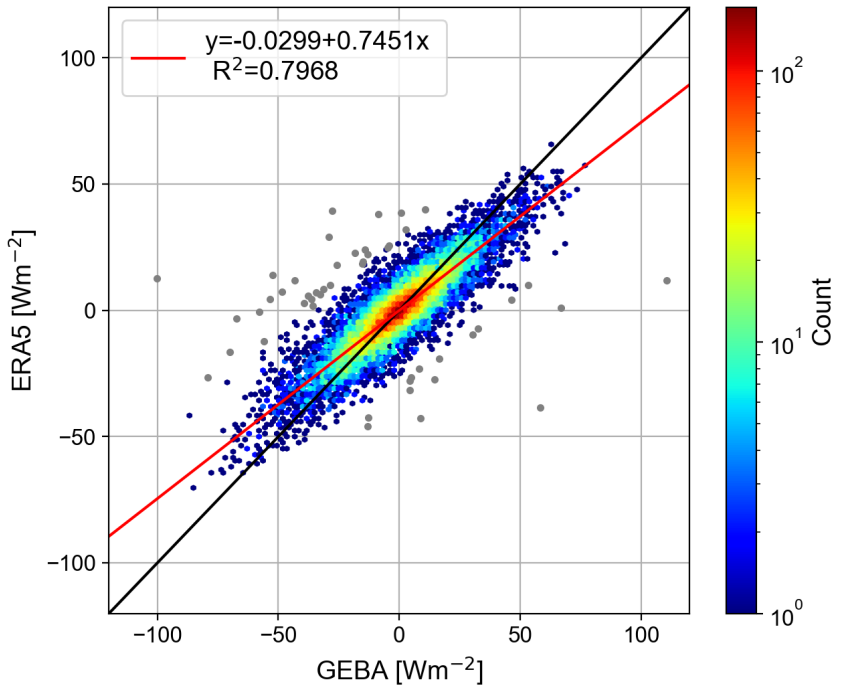

Figure: Scatter plot of ERA5 versus ground-based measurements of SSR deseasonalised, detrended anomalies over the period 1994-2019.

5. Current SSR trend

- Trend maps show a **widespread increase in SSR** during the period 1994-2019 for both GEBA and Solargis datasets.

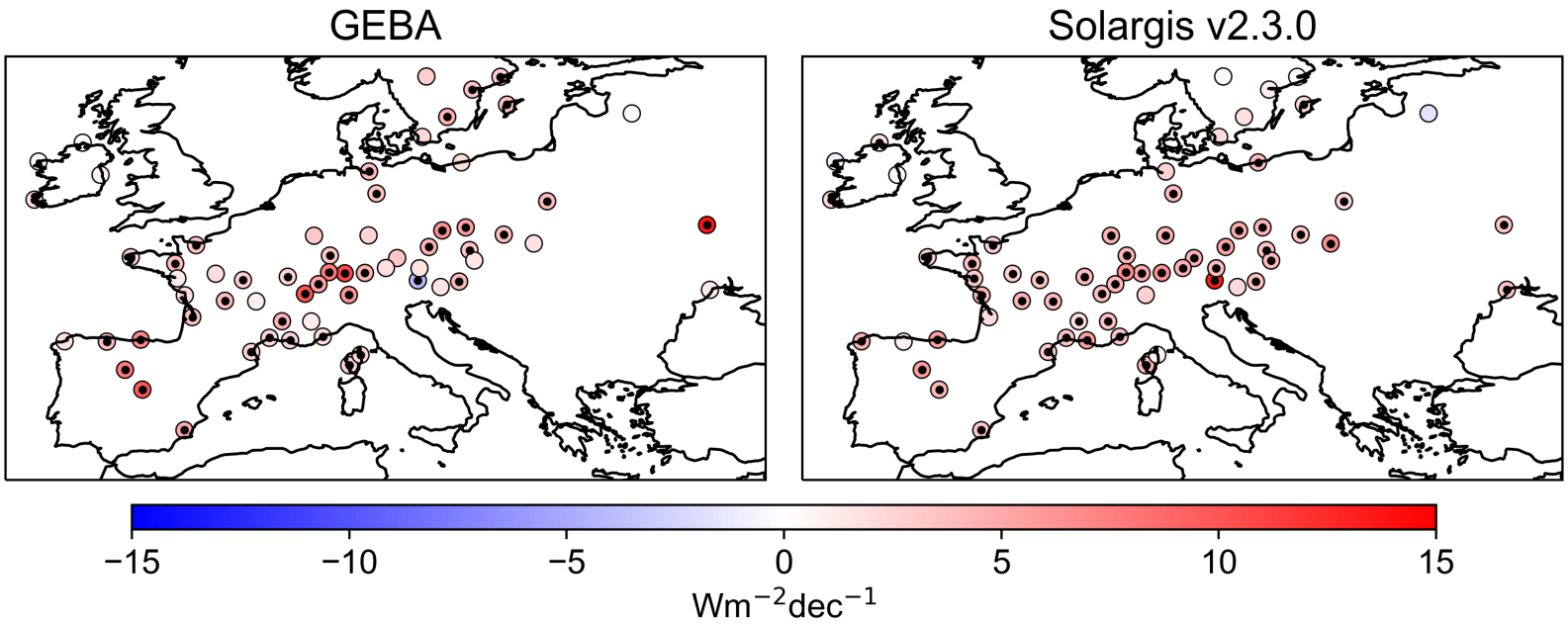

Figure: Linear trends of the monthly ground-observed (left) and satellite-derived (right) SSR series over Europe during the period 1994-2019. Significant trends ($p<0.05$) have been marked with black dots.

5. Current SSR trend

- **Wide-area average** trend rates for the period 1994-2019.

Table: Average SSR trends (Wm^{-2} per decade and %) for all datasets during the period 1994-2019.

Dataset	**% (Wm^{-2}) dec^{-1}** $\pm \sigma$
GEBA	**2.48 (3.48)** $\pm$ 1.98 (2.78)
SGv2.3.0	**2.45 (3.44)** $\pm$ 1.51 (2.12)
ERA5	1.11 (1.61) $\pm$ 0.84 (1.22)
CMIP6	0.89 (1.31) $\pm$ 0.40 (0.59)

- **ERA5** and **CMIP6** datasets show positive yet **significantly lower** average trends, as compared to those of GEBA an Solargis.

5. Current SSR trend

- Wide-area **average series** from satellite-based estimations **matches** the observational series accurately.

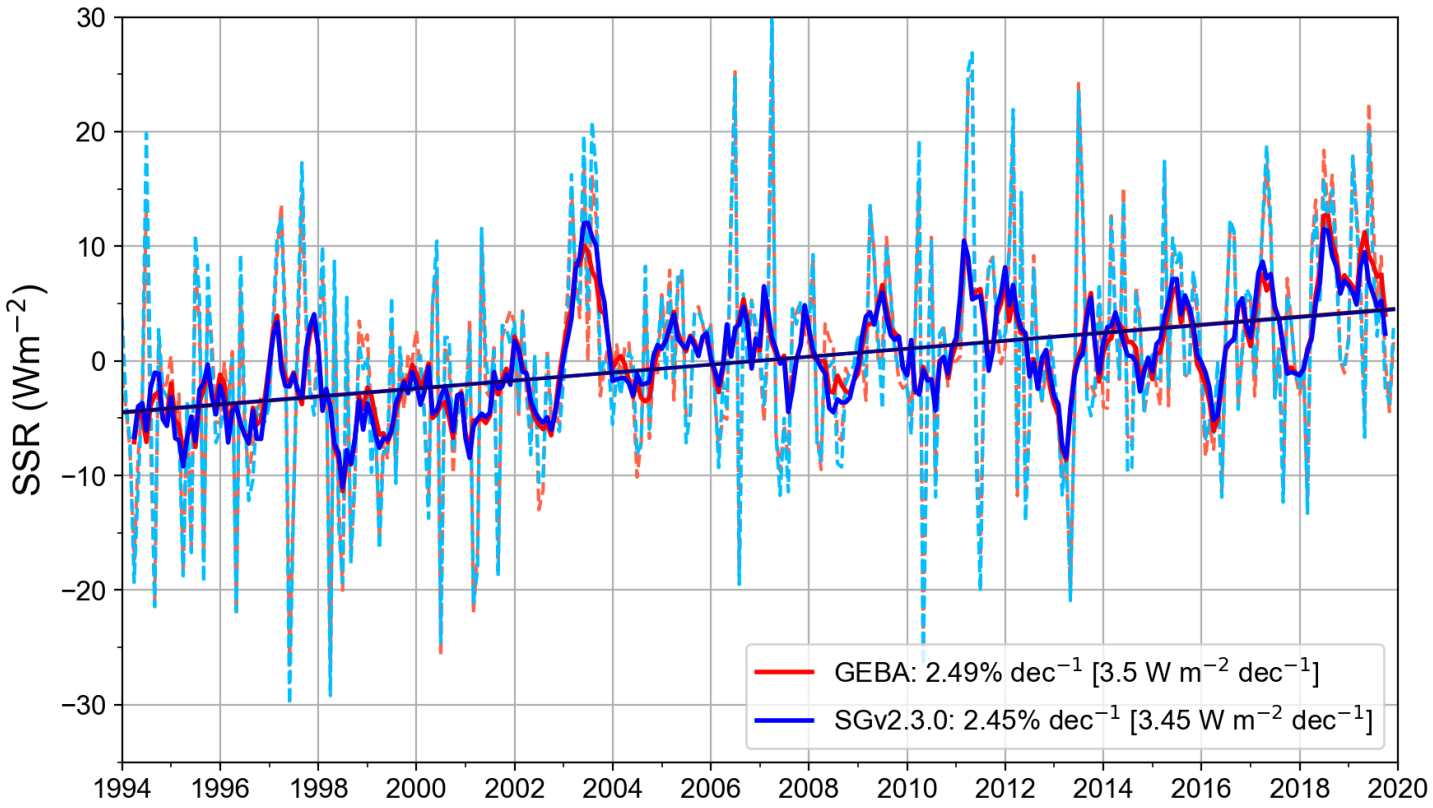

Figure: Monthly SSR deseasonalised anomaly series (dashed lines) of satellite-based (blue) and ground-measured (red) datasets, their 6-month centred moving average series (solid lines) and their trends (straight lines).

5. Current SSR trend

- Same plot with the **ERA5** and **CMIP6** datasets.

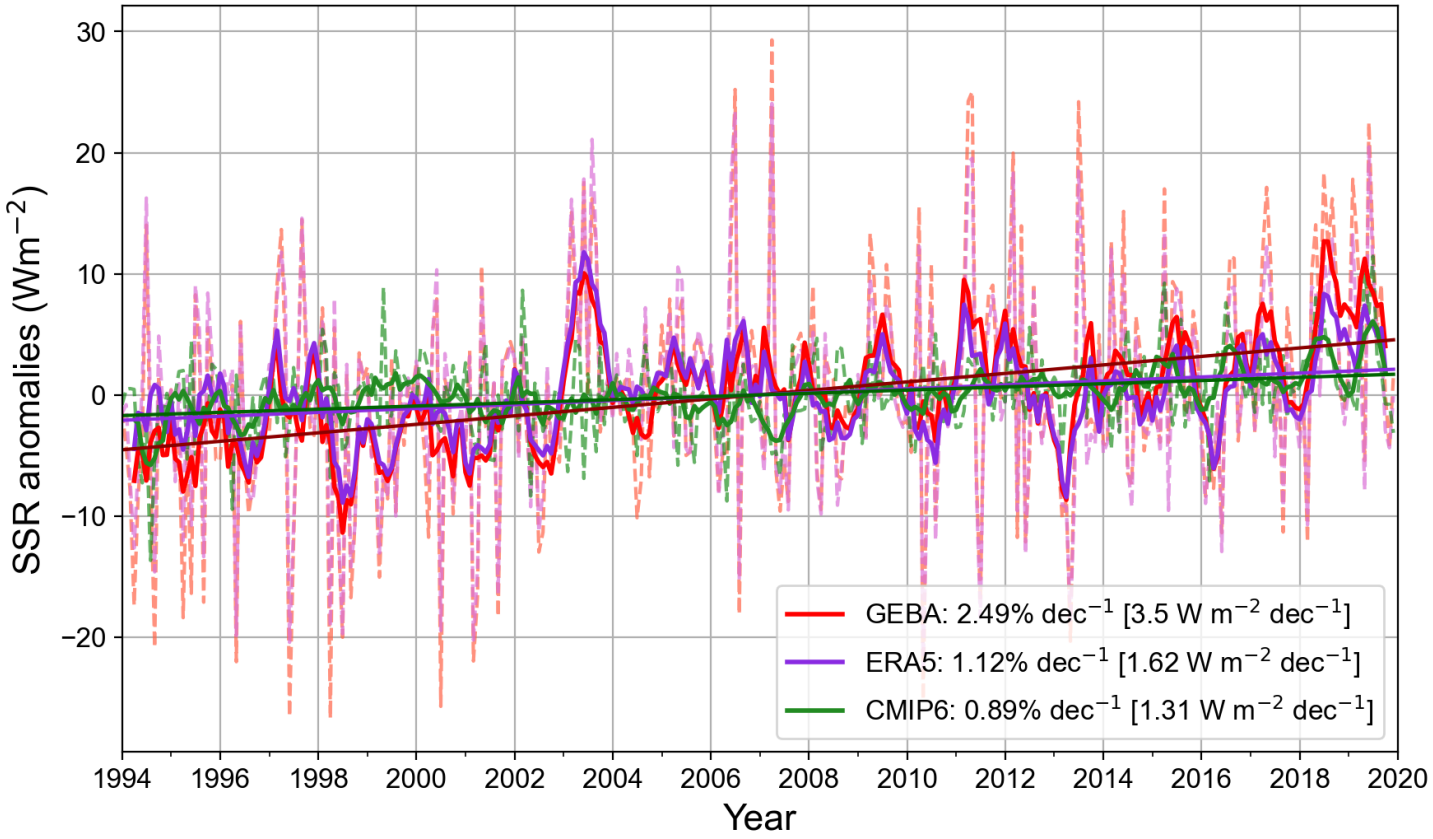

Figure: Monthly SSR deseasonalised anomaly series (dashed lines) of satellite-ground-measured (red), ERA5 reanalysis (purple) and average ensemble CMIP6 (green) datasets, their 6-month centred moving average series (solid lines) and their trends (straight lines).

5. Current SSR trend

- A similar analysis has been conducted for the **seasonal series**.

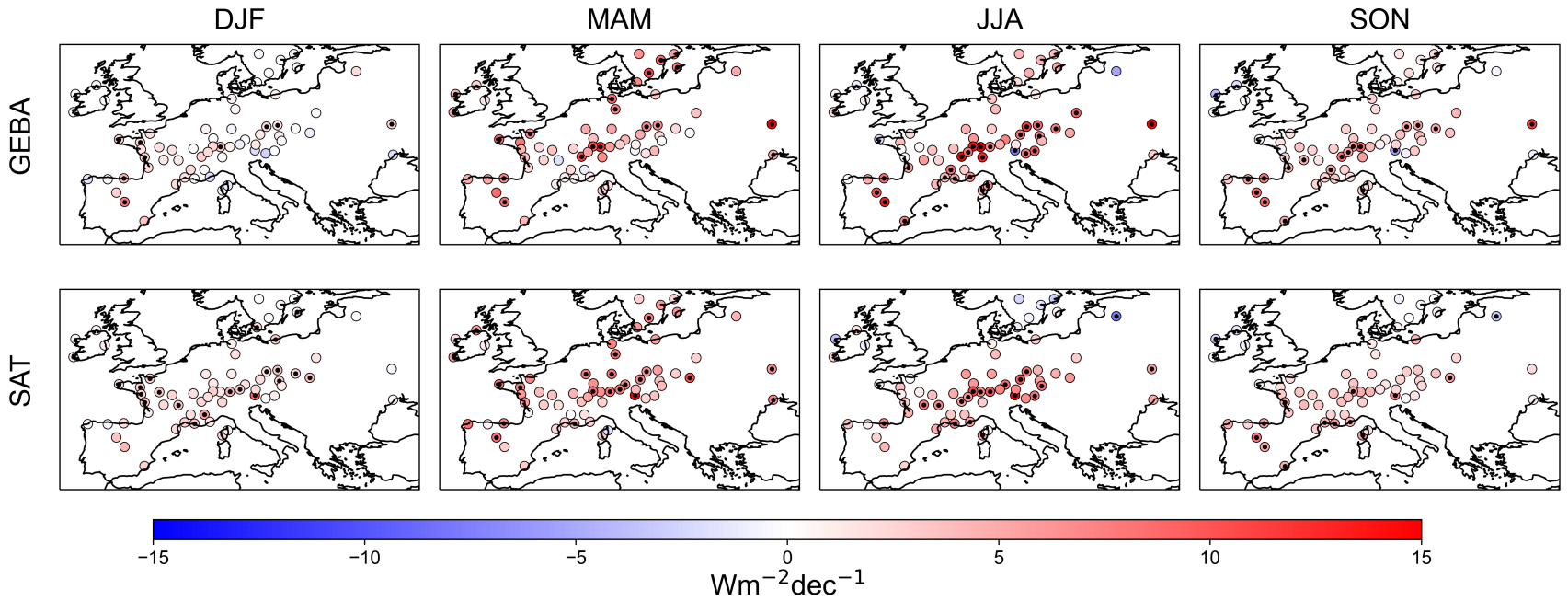

Figure: Seasonal trends of the monthly ground-observed (up) and satellite-derived (down) SSR series over Europe during the period 1994-2019. Significant trends ($p<0.05$) have been marked with black dots. Values are expressed as Wm^{-2} per decade.

5. Current SSR trend

Table: Average seasonal SSR trends (Wm^{-2} per decade) for all datasets during the period 1994-2019.

Dataset	DJF	MAM	JJA	SON
GEBA	0.84 ± 1.67	4.72 ± 3.53	5.44 ± 5.21	2.94 ± 2.94
SGv2.3.0	1.97 ± 1.52	5.12 ± 3.30	4.03 ± 3.83	2.65 ± 2.20
ERA5	-0.15 ± 1.01	2.12 ± 2.43	3.00 ± 2.99	1.49 ± 1.46
CMIP6	-0.14 ± 0.35	1.43 ± 1.16	3.25 ± 1.29	0.73 ± 0.57

- The **highest increases** in SSR are observed in **spring and summer**.
- **Low positive trend** in SSR during **winter**, or even negative trends in some stations.
- Satellite-based estimations use to slightly **over-predict** trends in winter and spring, and **under-predict** in summer and autumn.

5. Current SSR trend

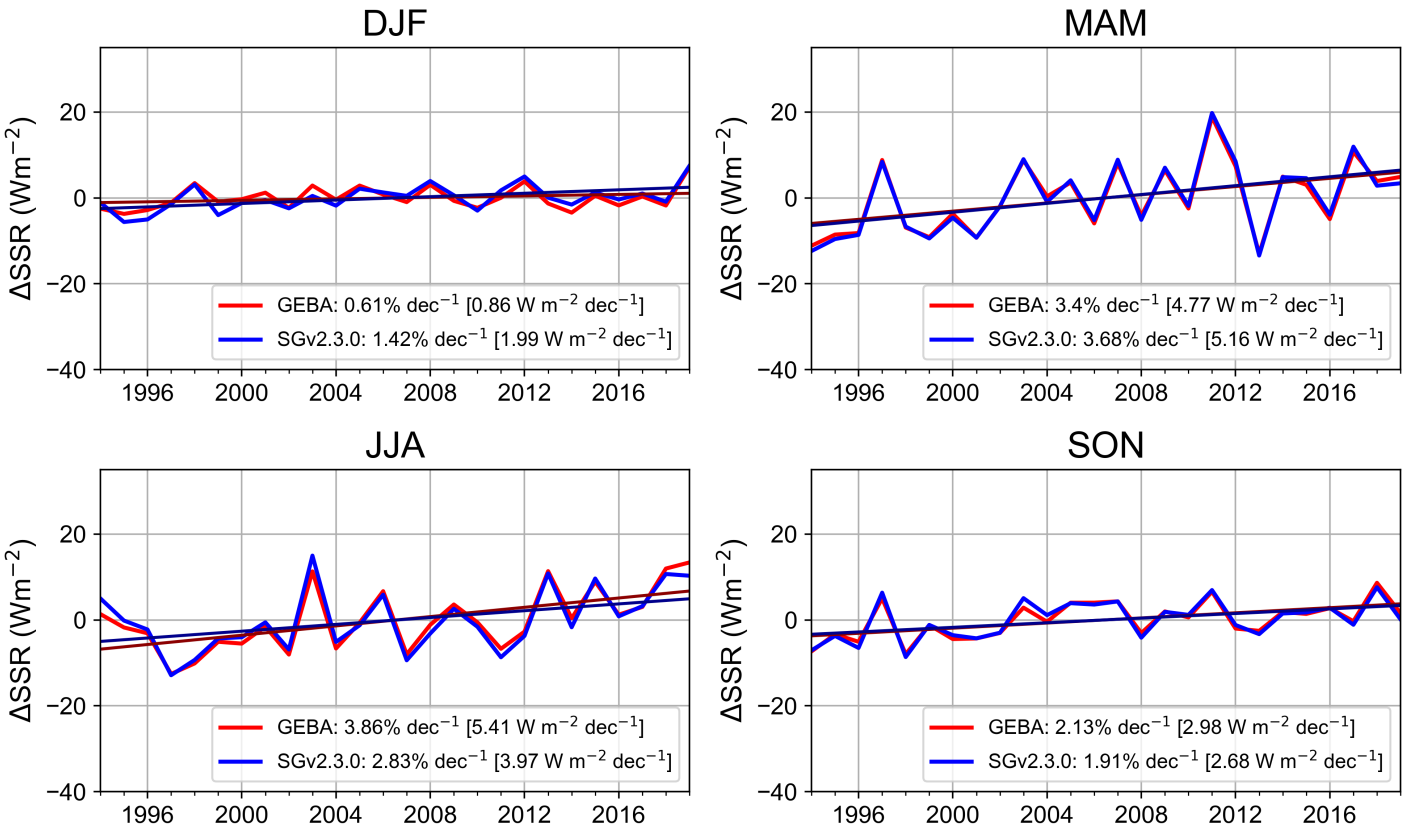

Figure: Seasonal SSR deseasonalised anomaly series of satellite-based (blue) and ground-measured (red) datasets. The series are expressed as anomalies (Wm^{-2}) from the 1994–2019 mean for each month separately.

6. Projected SSR trend

- All scenarios show **similar average trends** ($\sim$1 Wm^{-2} per decade).

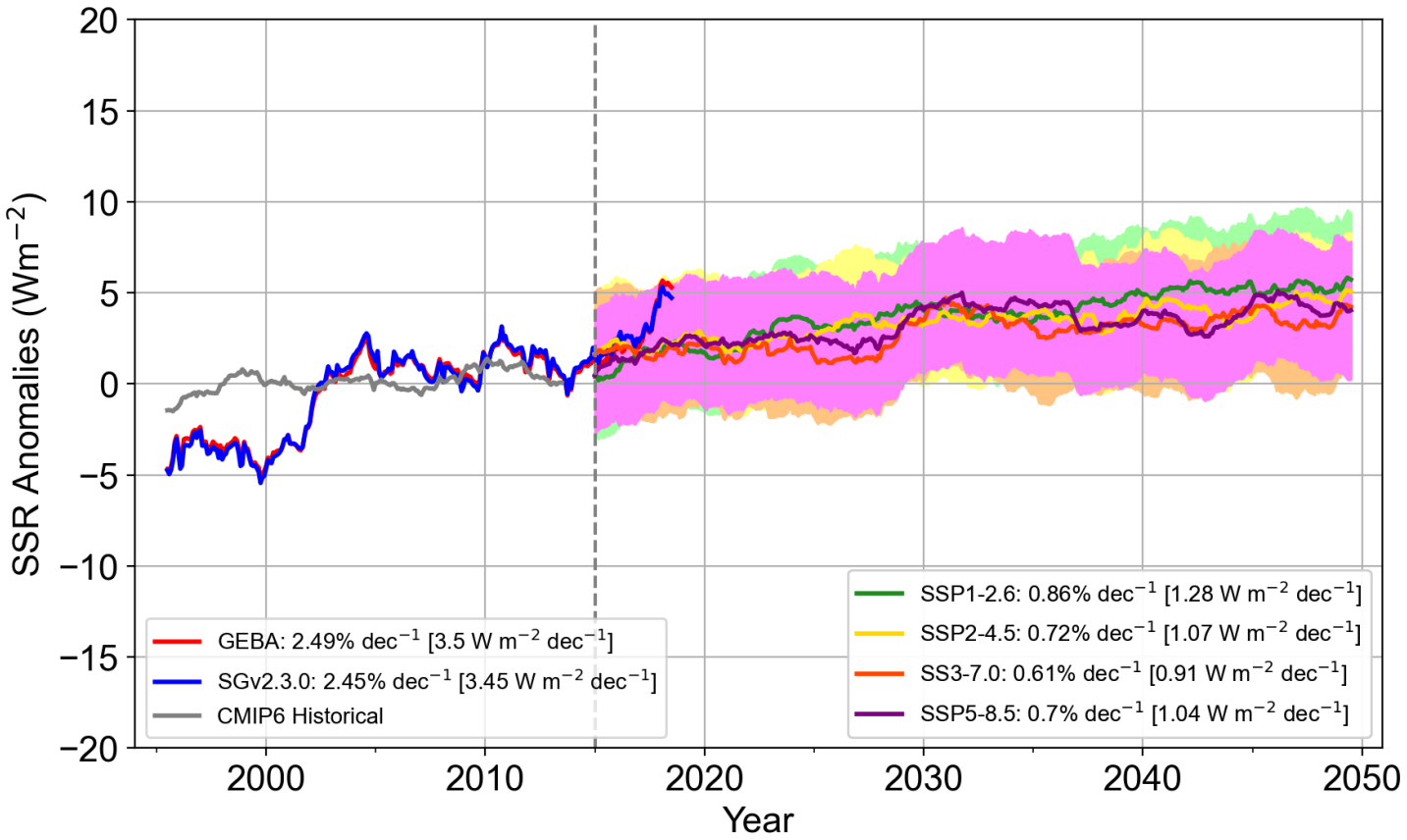

Figure: Monthly SSR deseasonalised anomaly series of satellite-based (blue) and ground-measured (red) for the period 1994-2019. Average CMIP6 for different CMIP6 models historical and SSP projection SSR series are plotted for the periods 1994-2014 and 2015-2050, respectively. The series are expressed as anomalies (Wm^{-2}) from the 1994–2019 mean for each month separately. Color envelopes represent the standard deviation of all models for each scenario.

7. Conclusions

First, SSR from **satellite-based** estimations have been **compared** to **measures** from 64 ground-based stations across Europe. Results show that:

1. There is an **excellent agreement** between ground observations and satellite-based SSR. Satellite-based estimations are able to reproduce approximately **94.8%** of the variability of the SSR measured by ground-based observations.
2. **Trend** analysis showed a **widespread increase in SSR** in Europe since 1994, with the highest rates of increase present in the central and southern regions of Europe.
3. Trends in satellite and ground-based data overlap properly in space and have almost identical **mean rates** of about **2.5% (3.5 $\mathbf{Wm^{-2}}$) per decade**.
4. Results of the **seasonal trends** study show that:
   - The **highest increases** in SSR are observed in **spring** and **summer**.
   - There was almost **no trend** in SSR during **winter**, or even a negative trend in some stations.
   - Satellite-based estimations slightly over-predict trends in winter and spring, and under-predict in summer and autumn.

7. Conclusions

Second, satellite and ground-based datasets have been compared to monthly SSR outputs from **ERA5** reanalysis and **CMIP6 model means** from different SSP's, for the same temporal period:

5. All SSP **scenarios show similar trends** in SSR.
6. Projections show a slight **increase in SSR** of about **1 Wm^{-2} per decade** until **2050**, with an increasing annual variability.
7. Overall, the **reliability** of these models is **inferior** to that of satellite-based data, suggesting that there are still **uncertainties** with regard to climate models SSR prediction.

Thanks for your attention

e-mail: leandrocristian.segadom@um.es

References I

Eyring, V., Bony, S., Meehl, G. A., Senior, C. A., Stevens, B., Stouffer, R. J., and Taylor, K. E. (2016). Overview of the coupled model intercomparison project phase 6 (CMIP6) experimental design and organization. *Geoscientific Model Development*, 9(5):1937–1958.

Gilgen, H. and Ohmura, A. (1999). The global energy balance archive. *Bulletin of the American Meteorological Society*, 80(5):831–850.

Gilgen, H., Wild, M., and Ohmura, A. (1998). Means and trends of shortwave irradiance at the surface estimated from global energy balance archive data. *Journal of Climate*, 11(8):2042–2061.

Global Solar Atlas (2019). Validation Report for Global Solar Radiation Model. `https://documents1.worldbank.org/curated/en/507341592893487792/pdf/Global-Solar-Atlas-2-0-Validation-Report.pdf`.

Hersbach, H., Bell, B., Berrisford, P., Hirahara, S., Horányi, A., Muñoz-Sabater, J., Nicolas, J., Peubey, C., Radu, R., Schepers, D., et al. (2020). The ERA5 global reanalysis. *Quarterly Journal of the Royal Meteorological Society*, 146(730):1999–2049.

Ineichen, P. (2013). Long term satellite hourly, daily and monthly global, beam and diffuse irradiance validation. interannual variability analysis. Technical report. ID: unige:29606.

Kendall, M. G. (1948). Rank correlation methods.

Lee, J., Marotzk, J., Bala, G., Cao, L., Corti, S., Dunne, J., Engelbrecht, F., Fischer, E., Fyfe, J., and Jones, C. (2022). 2021: Future global climate: Scenario-based projections and nearterm information.

Perez, R., Schlemmer, J., Kankiewicz, A., Dise, J., Tadese, A., and Hoff, T. (2017). Detecting calibration drift at ground truth stations a demonstration of satellite irradiance models' accuracy. In *2017 IEEE 44th Photovoltaic Specialist Conference (PVSC)*, pages 1104–1109. IEEE.

Pfeifroth, U., Sanchez-Lorenzo, A., Manara, V., Trentmann, J., and Hollmann, R. (2018). Trends and variability of surface solar radiation in Europe based on surface-and satellite-based data records. *Journal of Geophysical Research: Atmospheres*, 123(3):1735–1754.

Pinker, R., Zhang, B., and Dutton, E. (2005). Do satellites detect trends in surface solar radiation? *Science*, 308(5723):850–854.

Sanchez-Lorenzo, A., Enriquez-Alonso, A., Wild, M., Trentmann, J., Vicente-Serrano, S. M., Sanchez-Romero, A., Posselt, R., and Hakuba, M. Z. (2017). Trends in downward surface solar radiation from satellites and ground observations over Europe during 1983–2010. *Remote Sensing of Environment*, 189:108–117.

References II

Sanchez-Lorenzo, A., Wild, M., and Trentmann, J. (2013). Validation and stability assessment of the monthly mean CM SAF surface solar radiation dataset over europe against a homogenized surface dataset (1983–2005). *Remote sensing of environment*, 134:355–366.

Šúri, M. and Cebecauer, T. (2014). Satellite-based solar resource data: Model validation statistics versus user's uncertainty. In *ASES SOLAR 2014 Conference, San Francisco*, pages 7–9.

Wambui, G. D., Waititu, G. A., and Wanjoya, A. (2015). The power of the pruned exact linear time (pelt) test in multiple changepoint detection. *American Journal of Theoretical and Applied Statistics*, 4(6):581.

Wild, M., Folini, D., Hakuba, M. Z., Schär, C., Seneviratne, S. I., Kato, S., Rutan, D., Ammann, C., Wood, E. F., and König-Langlo, G. (2015). The energy balance over land and oceans: an assessment based on direct observations and CMIP5 climate models. *Climate Dynamics*, 44:3393–3429.

Wild, M., Ohmura, A., Schär, C., Müller, G., Folini, D., Schwarz, M., Hakuba, M. Z., and Sanchez-Lorenzo, A. (2017). The Global Energy Balance Archive (GEBA) Version 2017: A database for worldwide measured surface energy fluxes. *Earth System Science Data*, 9(2):601–613.

Appendix: average trend calculation methods

The calculation of the region-wide SSR trend was performed with 3 different methods:

- **Method 1** First calculate the average SSR time series throughout all considered sites, then calculate the deseasonalised anomalies of the average SSR time series, and finally compute the trend by linear fitting
- **Method 2** First calculate the deseasonalised anomalies site by site, then obtain the trend by linear fitting site by site, and finally obtain the average trend.
- **Method 3** Calculate the deseasonalised anomalies for each site, then calculate the average anomaly throughout all considered sites and finally compute the trend by linear fitting of the averaged anomaly.

Appendix: selected CMIP6 models

Table: Selected CMIP6 models and their main features. Source: `https://www.cesm.ucar.edu/community-projects/mmlea`

Modeling Center	Model Version	Model Resolution (atm/ocn)	Initialization Method	Forcing (Number of Members)	Reference (*ESGF reference)
CCCma	CanESM5	$\sim 2.8^\circ \times 2.8^\circ / \sim 1.4^\circ \times 0.9^\circ$	Macro	historical (50), ssp126 (50), ssp245 (50), ssp370 (50), ssp585 (50)	Swart et al. (2019)
CNRM	CNRM-CM6-1	$\sim 1.4^\circ \times 1.4^\circ$/nominal 1°	Macro	historical (30), ssp126 (6), ssp245 (10), ssp370 (6), ssp585 (6)	*Voldoire (2018)
EC-Earth Consortium	EC-Earth3	$\sim 0.7^\circ \times 0.7^\circ$/nominal 1°	Macro	historical (23), ssp126 (7), ssp245 (5), ssp370 (7), ssp585 (7)	*EC-Earth Consortium (2019)
NASA	GISS-E2-1-G	$\sim 2^\circ \times 2.5^\circ / \sim 1^\circ \times 1.25^\circ$	Macro	historical (40), ssp126 (2), ssp245 (15), ssp370 (2), ssp585 (2)	*NASA GISS (2019)
Met Office	UKESM1-0-LL	$\sim 1.25^\circ \times 1.9^\circ$/nominal 1°	Macro	historical (17), ssp126 (5), ssp245 (5), ssp370 (5), ssp585 (5)	*Tang et al. (2019)
MIROC	MIROC6	$\sim 1.4^\circ \times 1.4^\circ$/nominal 1°	Macro	historical (50), ssp126 (50), ssp245 (50), ssp370 (3), ssp585 (50)	Tatebe et al. (2019)

Appendix: selected GEBA sites

No.	Station	Country	Longitude (º)	Latitude (º)	No.	Station	Country	Longitude (º)	Latitude (º)
1	Sonnblick	AT	12.95	47.05	**33**	Ajaccio	FR	8.80	41.92
2	Graz	AT	15.45	46.98	**34**	Malin Head, C.	IE	-7.33	55.37
3	Klagenfurt	AT	14.33	46.65	**35**	Belmullet	IE	-10.00	54.23
4	Locarno-Monti	CH	8.78	46.17	**36**	Dublin Airport	IE	-6.25	53.43
5	Hradec Kralove	CZ	15.85	50.25	**37**	Valentia	IE	-10.25	51.93
6	Ostrava-Poruba	CZ	18.15	49.82	**38**	Kolobrzeg	PL	15.58	54.18
7	Churanov	CZ	13.62	49.07	**39**	Belsk	PL	20.78	51.83
8	Kucharovice	CZ	16.08	48.88	**40**	Zakopane	PL	19.97	49.28
9	Braunschweig	DE	10.45	52.3	**41**	Stockholm	SE	17.95	59.35
10	Wuerzburg	DE	9.97	49.77	**42**	Kiev	UA	30.45	50.40
11	Trier	DE	6.67	49.75	**43**	Odessa	UA	30.63	46.48
12	Weihenstephan	DE	11.70	48.40	**44**	Wien-Hohe-Warte	AT	16.37	48.25
13	Hohenpeissenberg	DE	11.02	47.8	**45**	Praha / (Prag-Karlov)	CZ	14.43	50.07
14	Santander	ES	-3.82	43.47	**46**	Zuerich-Kloten	CH	8.53	47.48
15	Oviedo	ES	-5.87	43.35	**47**	Hamburg	DE	10.00	53.63
16	Madrid	ES	-3.72	40.45	**48**	Bastia	FR	9.48	42.55
17	Murcia	ES	-1.17	38.00	**49**	Karlstad	SE	13.47	59.37
18	Caen	FR	-0.47	49.18	**50**	Lund	SE	13.22	55.72
19	Strassburg	FR	7.63	48.55	**51**	Norrkoepping	SE	16.25	58.58
20	Rennes	FR	-1.73	48.07	**52**	Vaexjoe / Kronoberg	SE	14.73	56.93
21	Tours	FR	0.72	47.45	**53**	Visby - Aerolog. Station	SE	18.35	57.67
22	Dijon	FR	5.08	47.27	**54**	Basel	CH	7.58	47.55
23	Nantes	FR	-1.60	47.17	**55**	Brest	FR	-4.42	48.45
24	La Rochelle	FR	-1.15	46.15	**56**	Bourges	FR	2.37	47.07
25	Limoges	FR	1.28	45.82	**57**	Bregenz	AT	9.75	47.50
26	Clermont-Ferrand	FR	3.17	45.78	**58**	Salzburg / Freisal	AT	13.05	47.78
27	Bordeaux	FR	-0.70	44.83	**59**	La Coruna	ES	-8.42	43.37
28	Embrun	FR	6.50	44.57	**60**	Valladolid	ES	-4.77	41.65
29	Nice	FR	7.20	43.65	**61**	Montelimar	FR	4.73	44.58
30	Montpellier	FR	3.97	43.58	**62**	Zoseni	LV	25.90	57.14
31	Marignane	FR	5.22	43.43	**63**	Geneve-Cointrin	CH	6.12	46.24
32	Perpignan	FR	2.87	42.73	**64**	Payerne (BSRN)	CH	6.94	46.82

Appendix: GEBA, ERA5 and CMIP6 average series

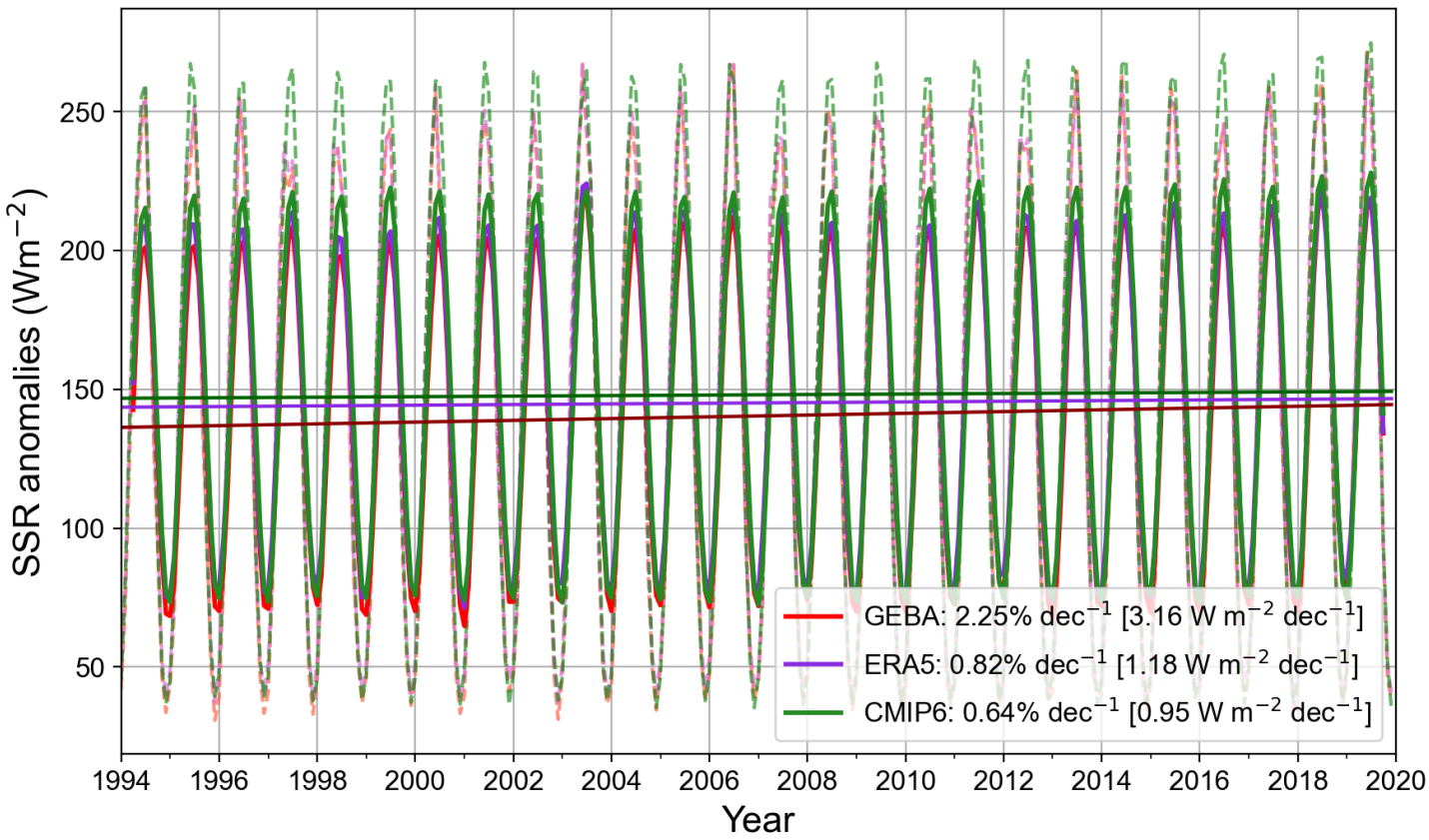

Figure: SSR series of ground-measured (red), ERA5 (purple) and CMIP6 (green) datasets. The series are expressed as Wm^{-2} for the 1994–2019 period, together with their respective linear trends.